

## RESEARCH ARTICLE

# Driver Injury During Automatic Emergency Steering in Vehicle–Vehicle Side-Impact Collisions

CHENGLONG ZHANG<sup>1</sup>, XIAOYAN LI<sup>2</sup>, YI LEI<sup>1</sup>, DAOWEN ZHANG<sup>1,3</sup>, AND TIANSHU ZHANG<sup>4</sup><sup>1</sup>School of Automobile and Transportation, Xihua University, Chengdu 610039, China<sup>2</sup>Chengdu Metro Operations Company, Chengdu 610066, China<sup>3</sup>Vehicle Measurement Control and Safety Key Laboratory of Sichuan Province, Xihua University, Chengdu 610039, China<sup>4</sup>Engineering, Computer and Mathematical Sciences, The University of Adelaide, Adelaide, SA 5005, Australia

Corresponding author: Daowen Zhang (0119910025@mail.xhu.edu.cn)

This work was supported in part by the Depth Investigation and Safety Analysis of Vehicle Accidents in Typical Cities and Mountainous Areas under Grant 222304, and in part by the In-Depth Investigation and Prevention of Electric Two-Wheeled Vehicle Accidents in Sichuan under Grant 172487.

**ABSTRACT** Automatic emergency steering (AES) is an advanced assisted driving system. AES systems help avoid collisions by controlling the lateral movement of a vehicle. However, in some scenarios—such as those involving a laterally approaching vehicle that cannot be detected by AES sensors owing to the vehicle's obstruction by an obstacle—AES systems do not have sufficient time to act, and side impact may still occur. Limited research has been conducted on driver impairment analysis under the influence of AES. This study investigated driver kinematic responses and injuries after side impact following the AES. First, the study was based on accident cases in the National Automobile Accident In-Depth Investigation System database; a precrash scenario involving AES was established using the PreScan software. Second, a finite element model subjected to side impact was established in HyperMesh; a validated driver restraint system was added to the model. The effects of the impact angle, impact location, and ride posture on driver responses and injuries were investigated. It appears that as the impact angle increases, the forces on the abdomen tend to decrease. When the impact angle is 60°, the abdominal combined force *APF* is 2638N, which exceeds the threshold value. We have got the weighted injury criterion (*WIC*) for five angles: 60°, 75°, 90°, 105°, and 120°. Their values are 0.485, 0.393, 0.408, 0.200, and 0.158. The impact location had *WIC* values of 0.230, 0.407, and 0.228 for pillars A, B, and C, respectively; the *WIC* values for normal and left-toward positions were 0.492 and 0.407 respectively. Finally, the effects of an active seat belt pre-tensioning system on driver responses and injuries under various lateral accelerations were also investigated. These results contribute to a reference for investigating scenarios of AES or integrated technology of vehicle active and passive safety.

**INDEX TERMS** AES, driver kinematic responses, driver injury, finite element, side impact.

## I. INTRODUCTION

Automatic emergency steering (AES) is an advanced assisted driving system that can improve safety under certain driving scenarios [1]. The European New Car Assessment Protocol (Euro-NCAP) plans to include AES system functions in its testing in 2025 [2]. AES systems can reduce the probability of collisions [3], [4]; nevertheless, if a vehicle is in a blind spot in the detection area of AES system sensors, the AES systems may have insufficient time to act, and a collision may still occur [5]. AES systems can reduce accident severity in

crashes, and injury prevention efforts are transitioning from a focus on fatalities and serious injuries to including less severe collisions, studying crashes in the presence of AES systems can further enhance driver safety environments and reduce driver injuries. According to statistics from the United States, side impact constituted 33% of all vehicle–vehicle collisions, and its probability of occurrence was second only to the frontal collision [6]. Moreover, a Chinese annual report of traffic accident statistics from 2001 to 2015 revealed that among 11 211 car collisions, 27% involved side impacts [7]. In vehicle design, relatively few vehicle parts can absorb energy during side impact, and the survival space of vehicle occupants is easily reduced or compromised; thus, this

The associate editor coordinating the review of this manuscript and approving it for publication was Wei Wei<sup>1</sup>.

increases the likelihood of the occupants sustaining severe injuries during side impact. And side impacts are more complex than frontal collisions [8]. With the promotion of lightweight vehicle structures, the energy absorption characteristics of the body structure as well as occupant injuries have attracted wide attention, and many scholars have studied the vehicle structure, but there are fewer studies involving driver injuries. Although active safety technology can compensate for driver error to some extent and act as a driving aid, it does not completely prevent driver injury. When an accident cannot be avoided, it becomes especially important to minimize driver injuries. The greater the intrusion into the doors and B-pillars during a collision, and the smaller the survivability of the occupants, the more severe the injury will be, and studying collisions in AES scenarios to reduce this injury will make the driver as safe as possible. AES systems have been demonstrated to cause an apparent displacement of both the driver and other vehicle occupants when activated [9], and the degree of lateral displacement of the driver and occupant is related to the intensity of the AES-initiated vehicle motion [10]. Such displacement reduces the performance of conventional restraint systems for preventing occupant injury. This driver out-of-position (OOP) phenomenon renders the original restraint system ineffective in protecting the driver and occupant, resulting in increased driver and occupant injuries [11]. Accordingly, studying AES during side impact is critical for improving occupant protection.

Currently, the research direction of AES systems is mainly to optimize and improve them. AES systems mainly use sensors to perceive the vehicle's driving environment and assist the driver in maneuvering the car. Path planning and trajectory tracking are integral tasks in AES systems. The methods commonly used for AES path planning include the geometric curve, search, and artificial potential field methods [12]. The search method is to search all surrounding paths to obtain clusters of suitable trajectories, and it then determines the optimal path by using an objective function and constraints. However, the method has poor real-time performance [13]. Yang [14] compared the performance of multiple lane-change trajectory models and found that the model of a fifth-degree polynomial had the best performance. Mages et al. [16] developed an algorithm for bypassing obstacles during lane changes; they implemented this algorithm by increasing the order of a fifth-degree polynomial, and they determined that their algorithm exhibited superior real-time performance compared to other algorithms.

Nowadays, research primarily focuses on the combination of AEB with vehicle-vehicle collisions and the integration of AES with frontal and rear-end collisions. However, there is limited research on the combination of AES with side collisions, and some studies show that AES has a higher collision avoidance efficiency than AEB. Battaglia et al. [9] investigated vehicle emergency steering simulation experiments to conclude that vehicle seat characteristics, interior trim shape, and body size of the dummy model affect occupant displacement from the seat. Mages et al. [16] based

on a frontal collision with an AES system, concluded that occupants are displaced laterally during steering and that a change in occupant position leads to a change in their level of injury. During an automobile side impact, the driver's horizontal living space is negatively correlated with the injury. Xiao et al. [17] conducted tests of side impacts and oblique side impacts by using a Global Human Body Models Consortium model and a Toyota Camry model. They observed that distal oblique side impacts and side impacts resulted in more severe chest injuries in occupants than proximal impacts.

According to the preceding discussion, AES systems still cannot completely prevent collisions, and they cause lateral displacement of the driver and occupants, which reduces their survival space. Research on the effects of AES-induced driver out-of-position (OOP) on driver injuries during vehicle–vehicle collisions is insufficient. Nowadays, cars are basically assembled with an AES system, AES is one of the most important factors affecting the side impact, and at present the side impact of the AES system with the combination of the research is still small. To increase driver safety and improve research involving AES systems in side impacts, this study comprehensively examined the interrelationship between a vehicle's kinematic responses before a collision and those during a collision by considering both active and passive safety systems. Moreover, the study used multiple software programs to simulate AES functions in scenarios involving vehicle–vehicle side impact; the driver's OOP response and potential injuries in such scenarios were also analyzed. The results were used to develop an optimized restraint system that can reduce driver injury. The findings of this study not only provide a reference for the study of both active and passive safety systems and the optimal design of restraint systems but also contribute to efforts toward improving driver protection.

## II. MATERIALS AND METHODS

The side impact scenarios simulated in this study were based on real accident cases recorded in the National Automobile Accident In-Depth Investigation System (NAIS) database. Since this paper focuses on the study of intersection drooping driving conditions in vehicle-vehicle side-impact accidents, the selected accident case meets the following requirements: 1) the accident case involves only two passenger cars; 2) the target car relative to the direction of travel of the car is the left side of the oncoming car; 3) the accident case must be equipped with a car recorder or a surveillance video. According to the above screening process, a total of 46 relevant accident cases were statistically qualified. In this paper, we screened out the clear and typical side impact accidents of emergency steering of passenger cars at intersections under vertical driving conditions from these cases. An example scenario is depicted in Figure 1, and this accident is described as follows: The main car was traveling at a constant speed on a six-lane road with bidirectional traffic when the target car (red sedan) suddenly pulled out from the left into the main car lanes. When the main car detected the target car, the

AES system was activated to avoid a collision. However, the distance between the main car and the target car was excessively short, and the target car could not brake. Therefore, during the main car’s emergency steering maneuver to avoid the collision, the target car collided with the main vehicle’s B-pillar.

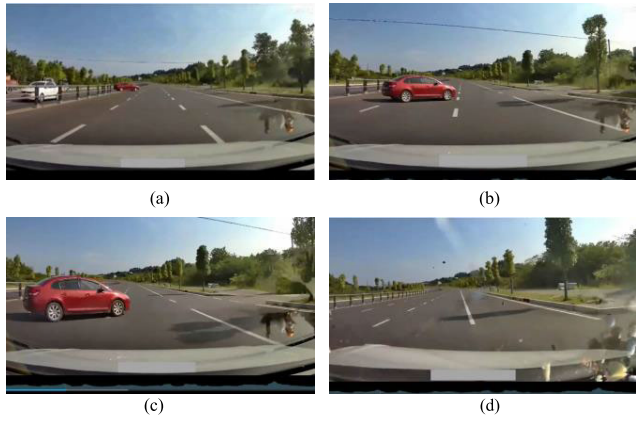


FIGURE 1. Stages of the accident case.

To accurately determine the vehicle’s kinematic response and occupant injuries, this study analyzed the evolution of this side impact while the vehicle’s AES was triggered. The vehicle’s kinematic responses before the collision and during the collision were evaluated. First, the vehicle’s kinematic response before the collision was obtained using PreScan, MATLAB/Simulink, and a CarSim cosimulation. Second, the vehicle’s kinematic response during the collision was obtained using HyperMesh and an LS-DYNA cosimulation. Finally, the kinematic responses before and during the collision were combined and input into a finite element model of the vehicle’s restraint system to analyze the kinematic responses of and total injuries to the driver during the collision.

**A. MODEL OF VEHICLE DYNAMICS**

**1) ESTABLISHMENT OF THE AES ALGORITHM**

An effective method for planning a lane-change trajectory should be simple, be applicable in real-time, and produce rational and continuous paths. According to research on drivers’ emergency steering, the lane-change trajectory for avoiding collisions during emergency steering approximates a fifth-degree polynomial [18]. Fifth-degree polynomials are widely used as lane-change trajectories because they are smooth and continuous curves that are similar to lane changes by humans [19]. An example trajectory is illustrated in Figure 2.

A fifth-degree polynomial can be expressed as follows:

$$y = \sum_{i=0}^5 c_i x^i = c_0 + c_1 x^1 + c_2 x^2 + c_3 x^3 + c_4 x^4 + c_5 x^5 \tag{1}$$

where  $x$  and  $y$  denote the longitudinal and lateral displacements of the lane change, respectively, and  $c_i$  denotes the

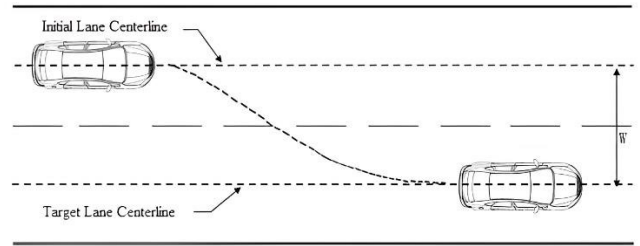


FIGURE 2. Collision avoidance trajectory.

coefficient of the fifth-degree polynomial. At the beginning of the lane change, the longitudinal starting point of the vehicle, lateral displacement, velocity, and acceleration are all zero. Let the lateral displacement and longitudinal displacement after the completion of the lane change be  $b$  and  $d$ , respectively; hence, the final reference trajectory based on these boundary conditions can be expressed as follows:

$$y = b \left[ 10 \left( \frac{x}{d} \right)^3 - 15 \left( \frac{x}{d} \right)^4 + 6 \left( \frac{x}{d} \right)^5 \right] \tag{2}$$

**2) SIMULATION SCENARIOS**

Based on the characteristics of typical real accident cases selected from the NAIS database, this study constructed a two-way four-lane intersection with a single-lane width of 3.75 m and a roadway adhesion coefficient of 0.8 by using the PreScan interface. The main car was considered to be equipped with an AES control module and to be driving at 60 km/h from west to east. The target car was considered to be driving at 50 km/h from north to south. Houses and other buildings occluded the target car; therefore, the main car’s sensors did not detect it. When the two cars reached the intersection, and the distance between them was already short, the main car’s sensors detected the target car from the lateral direction; at this time, emergency braking could not avoid the collision. Therefore, the AES control module triggered and applied emergency steering to avoid collision. However, the target car did not apply its brakes promptly, and because the two cars were too close, the main car collided with the side of the target car during its emergency steering maneuver. This scenario is depicted in Figure 3.

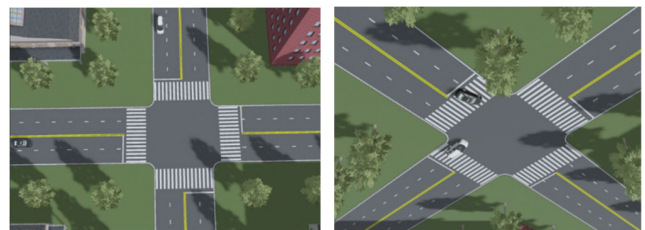


FIGURE 3. Simulation scenario.

CarSim was used to obtain the vehicle’s dynamics before the collision to perform the cosimulation of emergency steering at speeds of 50, 60, and 70 km/h. Figure 4 displays the

trajectory tracking results at each vehicle speed relative to the reference trajectory results planned by the fifth-degree polynomial. The trajectory tracking effect at different speeds is generally good, and the actual position curves at the three speeds are basically consistent with the reference trajectory curves.

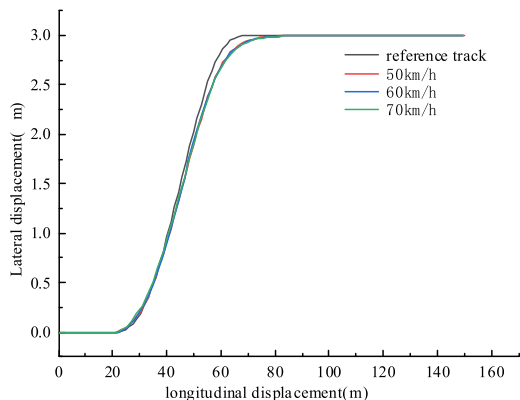


FIGURE 4. Vehicle emergency steering trajectories at different speeds.

**B. FINITE ELEMENT MODELING AND VALIDATION**

The base model for side impact in this study was a finite element model of a 2015 Camry vehicle that was developed by the National Center for Crash Analysis at the University of Washington. HyperMesh was used to establish the finite element model of the vehicle, and the LS-DYNA solver was used for the subsequent calculations. The finite element model had 2.25 million units and 1000 components, including the engine, chassis, suspension, steering, body, interior, and seat components. As presented in Table 1, the differences between the model and the real vehicle in terms of mass, rotational inertia, and center of gravity were <1%, <3%, and <3%, respectively. The total error between the real vehicle and the finite element vehicle model was within 5%, demonstrating the reliability of the finite element model. In the finite element model, a moving barrier was used instead of the target vehicle. The moving barrier model was a standard model provided by Livermore Software Technology Corporation (LSTC) [20], [21].

Based on HyperMesh finite element modeling platform was used to establish a finite element model of the side impact of the vehicle. To validate the accuracy of the finite element model, this study compared its collision simulation results with the results of the National Highway Transportation Safety Administration (NHTSA) NO.7517 real-vehicle collision test report. Referring to the collision test protocol to set the initial state of the collision, the test vehicle remains motionless, the speed of the moving barrier vehicle is set to 62km/h, and the collision angle of the two vehicles is set to 270°. Set the moving barrier to remain on the same level as the test vehicle, with the left edge probe of the moving barrier aligned with the reference line at the left front door edge of the test vehicle. As shown in Figure 5.

TABLE 1. Comparison of the simulated and real vehicle parameters.

Relevant parameters	real vehicle	simulated vehicle
quantity (kg)	1452	1462
Vehicle X-centered (mm)	1063	1086
Vehicle Y-centered (mm)	-9	-1
Vehicle Z-centered (mm)	561	560
pitch angle		
moment of inertia (kg*m <sup>2</sup> )	2519	2524
Transverse		
Pendulum Angular Moment of Inertia (kg*m <sup>2</sup> )	2796	2807
Lateral tilt angle		
moment of inertia (kg*m <sup>2</sup> )	560	572

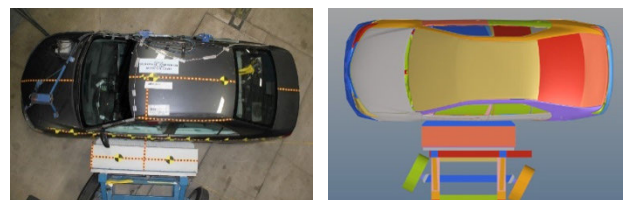
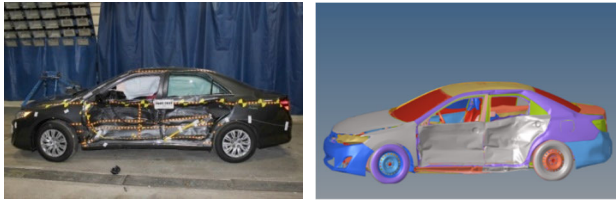


FIGURE 5. Initial collision position comparison.

The verification of the validity of the finite element model of the side-impact vehicle is mainly to compare the deformation parts and deformation amount of the vehicle and the moving barrier after the collision between the real vehicle test and the finite element simulation, and the acceleration curves of each part of the vehicle model after the collision are consistent with that of the real vehicle. As depicted in Figure 6, after the collision, the deformed parts on the impacted side of the finite element model were noted to be consistent with those in the real vehicle test. Specifically, these parts were the B-pillar, the window glass, the door sill beam, and the door on the driver’s side; the deformation of the door skin of the finite element model was also nearly identical to that of the real vehicle.



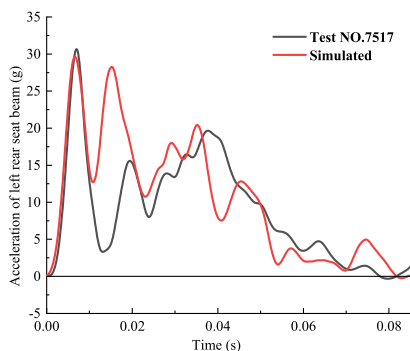
**FIGURE 6.** Comparison of impact damage for the simulated and real Camry vehicles.

As shown in Figure 7, a comparison of the results shows that the skin bumps on the left and right sides of the honeycomb aluminum at the front end of the mobile barriers of the simulation model, as well as the depressions in the middle, are basically the same as the deformation of the mobile barriers of the real vehicle.



**FIGURE 7.** Comparison of collision results of moving barriers.

In the No. NO.7517 real-vehicle test report on the NHTSA website, the acceleration curve for the B-pillar, and the acceleration data for the left-front seat beam are missing. Therefore, this study used the acceleration data for the left-rear seat beam for comparison and analysis. As illustrated in Figure 8, the maximum accelerations of the left-rear seat beam of the finite element model and real vehicle were 30.66g and 29.4567g, respectively, representing an error of 3.9%, which was determined to be within an acceptable range. Moreover, the time difference between the two curves was only 0.1 ms, and the overall trends of the acceleration curves obtained for the finite element model and the real vehicle were essentially the same.

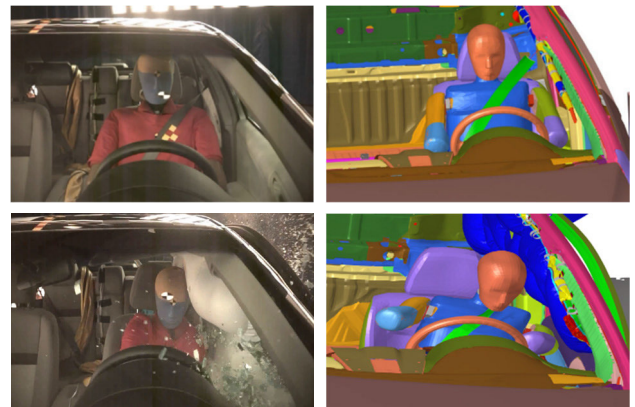


**FIGURE 8.** Simulated and actual acceleration curves of the left-rear seat crossbeam.

The deformation and acceleration curves of the whole vehicle in the simulation results were consistent, indicating

that the finite element model was reliable for simulating side impact.

The real-vehicle test report referenced in this paper was downloaded from the official website of NHTSA, and the real-vehicle crash test was provided by the U.S. Department of Transportation, so to improve the accuracy of the simulation test, the ES-2re dummy model similar to the real-vehicle test was selected. The total mass of this model is 73.338 kg with 427088 meshes, 301156 solid cells, 79 beam cells, and 20651 shell cells. Verify the effectiveness of the driver restraint system by referring to the Camry side impact test data published by NHTSA as NO.7517. According to the data provided in the experimental report, the distance of the dummy from the various parts of the vehicle, sitting posture, etc., is adjusted to ensure that the simulation model is consistent with the conditions of the real vehicle test before the collision. The main purpose of this paper is to see whether the dynamic response of the dummy in the collision stage in the simulation results is the same as the collision response process of the dummy in the real vehicle test, as well as to compare the damage curves of the dummies in Figure 9 show the comparison between the simulation model result animation and the real-vehicle test animation at the beginning and end moments of the collision, from which it can be seen that, at different collision moments, the tilting attitude of the dummy, the contact attitude between the dummy head and the side air curtains, the unfolding state of the side air curtains, as well as the contact between the torso of the body and the side door, are all in line with the real-vehicle test animation.



**FIGURE 9.** 0ms moment of collision and 100ms moment of collision.

As shown in Figure 10, comparing the occupant injury curves of the simulation test and the real vehicle test, the peak time of the two curves is basically the same, and the overall trend of the curves is basically the same as that of the real vehicle test, which indicates that the model has a certain degree of accuracy.

In summary, the reliability and validity of the model were verified through comparative experiments, and the results could be used in a subsequent analysis of driver injury.

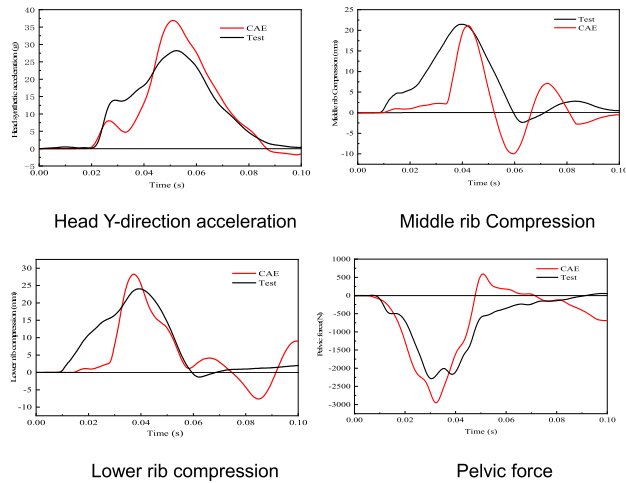


FIGURE 10. Driver injury comparisons.

C. DRIVER INJURY EVALUATION

In the event of a vehicle impact, despite the driver being protected by safety devices such as seat belts, side air curtains, and side airbags, it is still difficult to predict the injury resulting from a driver in motion colliding with the internal structure of the vehicle. Predicting these injuries is challenging. Therefore, during finite element simulations of collisions, sensors should be arranged in each part of the dummy to identify the damage to the corresponding part. This study used a finite element model of a dummy to mainly focus on driver head, chest, abdominal, and pelvic injuries. The following indices were used to evaluate injuries sustained by the dummy:

1) The head injury criterion (*HIC*) was used to assess occupant head injury:

$$HIC = (t_2 - t_1) \left[ \frac{1}{t_2 - t_1} \int_{t_1}^{t_2} R(t)dt \right]^{2.5}, t_0 \leq t_1 \leq t_2 \leq t_e \tag{3}$$

where  $t_0$  is the time at which the collision begins (s);  $t_e$  is the time at which the collision ends (s);  $t_1$  and  $t_2$  are the start and stop times for which the *HIC* value is maximized (s), respectively; and  $R(t)$  is the synthetic acceleration of the head (g).

2) The chest viscosity index (*VC*) was used to evaluate chest injuries:

$$VC = V(t) \cdot C(t) = \frac{d[D(t)]}{dt} \frac{D(t)}{D(0)} \tag{4}$$

where  $V(t)$  is the deformation velocity,  $C(t)$  is an instantaneous compression function, and  $D(t)$  is the deformation. A *VC* value of  $> 1.0$  m/s indicates a severe chest injury.

3) The abdomen peak force (*APF*) was used to evaluate abdominal injuries. *APF* is an index of the peak combined force on the abdomen. The *APF* threshold was 2500 N, and this index can be expressed as follows:

$$APF = \max |F_{FRONT-y} + F_{MIDDLE-y} + F_{BACK-y}| \tag{5}$$

4) Pelvic injuries were evaluated in terms of the force received at the pubic bone (pubic force); the threshold value for injury was 6000 N.

Each damage index indicates only the risk of damage to one part of the dummy. To evaluate the overall damage to the dummy, the weighted injury criterion (*WIC*) was used. The *WIC* is a weighted sum of the head, chest, abdominal, and pelvic damage and can be expressed as follows [22], [23]:

$$WIC = 0.3 \left( \frac{VC}{1.0} + \frac{RDC}{42} \right) + 0.2 \left( \frac{APF}{2.5} + \frac{PSPF}{6} \right) \tag{6}$$

where *VC* is the thoracic viscosity index (m/s), *RDC* is the thoracic rib-cage compression (mm), *APF* is the abdominal force (kN), and *PSPF* is the pubic force (kN).

D. SIMULATION EXPERIMENT

As mentioned, the vehicle’s kinematic responses before the collision and during the collision were evaluated. First, the vehicle’s kinematic response before the collision was obtained through a cosimulation conducted using PreScan, MATLAB/Simulink, and CarSim. Second, the vehicle’s kinematic response during the collision was obtained through a cosimulation conducted using HyperMesh and LS-DYNA. Finally, the kinematic responses before and during the collision were combined and input into the finite element model of the occupant restraint system to analyze the driver’s kinematic response and overall injuries during the collision. The entire process is illustrated in Figure 11.

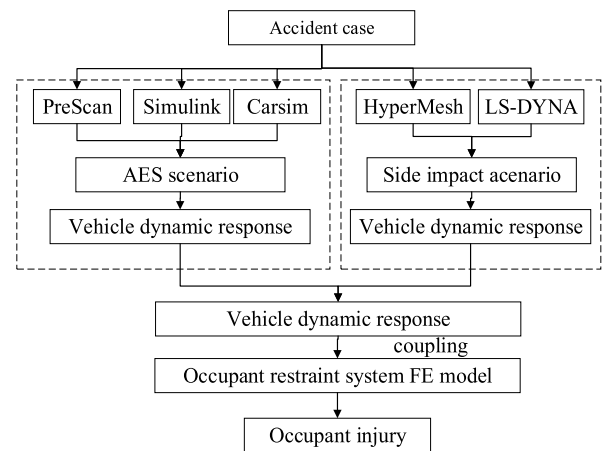


FIGURE 11. Flowchart for driver OOP analysis

The actual road environment is complex, and two-vehicle collisions can occur in numerous forms. After reviewing accident cases recorded in the NAIS database [24], this study identified three collision parameters—namely the AES action strength, the collision angle, and the collision position—and investigated their effects on the overall injuries sustained by the driver (Table 2).

These parameters were varied to identify the scenario with maximum driver injury, configure the active seat belt pre-tensioning system in the model, and analyze the effects

**TABLE 2.** Selected parameters.

factor	Parameters	Unit	realm
<i>A</i>	Strength of AES action	(g)	0.3-0.6
<i>B</i>	impact angle	(°)	60-120
<i>C</i>	collision position		A/B/C pillar

of active seat belt pre-tensioning on the driver’s kinematic response and injuries. The analysis results can provide a reference for designing an active restraint system.

**III. RESULTS**

**A. DRIVER KINEMATIC RESPONSE TO DIFFERENT LATERAL ACCELERATIONS**

Various lateral acceleration curves were extracted from the simulation of the constructed AES system and input to the finite element model to study the driver’s OOP response. According to the relevant literature, vehicles’ lateral acceleration during emergency steering should be at least 0.3g [25] and at most 0.67g [26]. Therefore, the lateral acceleration in the simulation model was set to 0.3g, 0.4g, 0.5g, or 0.6g. To ensure that the driver OOP response for each lateral acceleration was affected by only the acceleration profile, the initial positions of the main vehicle and the dolly were the same in all simulations, and the duration of all simulations was 0.5 s. Table 3 presents the kinematic response of the driver, wearing a traditional seat belt, to each lateral acceleration in three views; red, green, blue, and yellow indicate the OOP responses under lateral accelerations of 0.3g, 0.4g, 0.5g, and 0.6g, respectively. As indicated in the table, at 100 ms, the dummy postures for each lateral acceleration already differed, but the differences were only moderate. At 300 ms, the AES system was triggered, and the dummy was displaced to the left due to inertia; the differences in dislocation were relatively high. At 400 ms, the dummy’s displacements were maximized for all lateral accelerations; specifically, the head, chest, arms, and thighs all shifted toward the left, and their displacements were largest and smallest at the lateral accelerations of 0.6g and 0.3g, respectively.

Owing to the constraining effect of the seat belt, the displacements of the dummy’s chest and pelvis were small. The head and neck were less constrained by the seat belt, and they thus continued shifting toward the left during emergency steering. As listed in Table 4, at a lateral acceleration of 0.6g, the maximum head displacement was 136.753 mm, the maximum neck displacement was 92.395 mm, the maximum chest displacement was 54.791 mm, and the maximum pelvic displacement was 22.526 mm.

**B. ANALYSIS OF DRIVER INJURY FOR DIFFERENT SITTING POSTURES**

This study observed that when the AES system was activated, it resulted in a leftward OOP response in the driver. Does this lateral displacement have a new effect on the driver and does

**TABLE 3.** Dynamic response of the driver’s sitting posture under four lateral accelerations with a traditional seat belt.

Time	front view	left view	top view
100ms			
300ms			
400ms			
500ms			

it act as a cushion? To analyze whether this sitting position increases driver injuries, this study compared injuries sustained in a normal sitting position with those sustained in the AES-induced leftward sitting position at different moments during the collision (Table 5 ); the study considered the passive constraint system in this comparison.

As indicated in Table 5, at 60 ms into the collision, the dummy head had the greatest contact with the side air curtains; however, the degree of contact between the dummy and the side curtain is also different with different sitting postures. At 90 ms into the collision, the dummy head began to rebound because of the action of the side air curtains. At 150 ms into the collision (the late stage of the collision), the dummy head and torso both rotated; this rotation was greater in the AES-induced leftward sitting position, in which the entire car was at an angle about the collision direction. The dummy rotation and the parts and depths at which the dummy contacted the side air curtain differed between the normal and leftward sitting positions. The reason for this observation







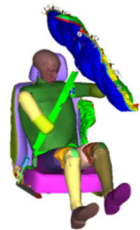
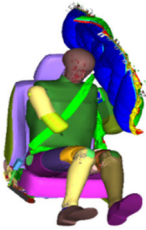
**TABLE 4. Maximum leftward (y-direction) displacement of the dummy for four lateral accelerations.**

	0.3g	0.4g	0.5g	0.6g
Maximum head displacement (mm)	105.234	113.515	122.914	136.753
Maximum neck displacement (mm)	80.027	81.844	83.450	92.395
Maximum chest displacement (mm)	47.810	48.834	50.493	54.791
Maximum pelvic bone displacement (mm)	24.593	23.301	21.206	22.526

is that the dummy was closer to the side air curtains in the AES-induced leftward sitting position. Moreover, the shoulder belt of the seat belt moved to the upper right side of the dummy and exhibited a tighter fit to the dummy’s shoulder and neck; hence, the seat belt could protect the dummy during a collision. The leftward OOP stance was caused by the angle of the side impact between the vehicle and the moving barrier during emergency steering. The vehicle has a certain angle during the collision, so that the collision deceleration is decomposed along the three directions of X, Y, and Z, and the vehicle deflects around the Z axis during the collision.

The synthetic acceleration of the dummy’s head reached its maximum value at 0.56 s for both sitting positions, and the HIC values were much smaller than the threshold values. The main reason is that although the contact position and attitude of the head and side air curtains are different in different seating positions, the side air curtains were able to unfold and wrap the head in time, and there was no collision with the window glass and other interior parts, so the head damage value was not large. The injury curves obtained for each body part of the dummy for each sitting position are presented in Figure 12. The curves obtained for upper rib-cage compression, middle rib-cage compression, and lower rib-cage compression in the dummy in the two sitting positions exhibited similar trends. The maximum compression levels of the lower rib cage were similar between the two positions and occurred at approximately 0.54 s. This is because, in the event of a side impact, the lower end of the dummy’s left arm comes into contact with the deformed door and is compressed by the door, transmitting the impact force to the chest. For the normal sitting position, the maximum compression and VC of

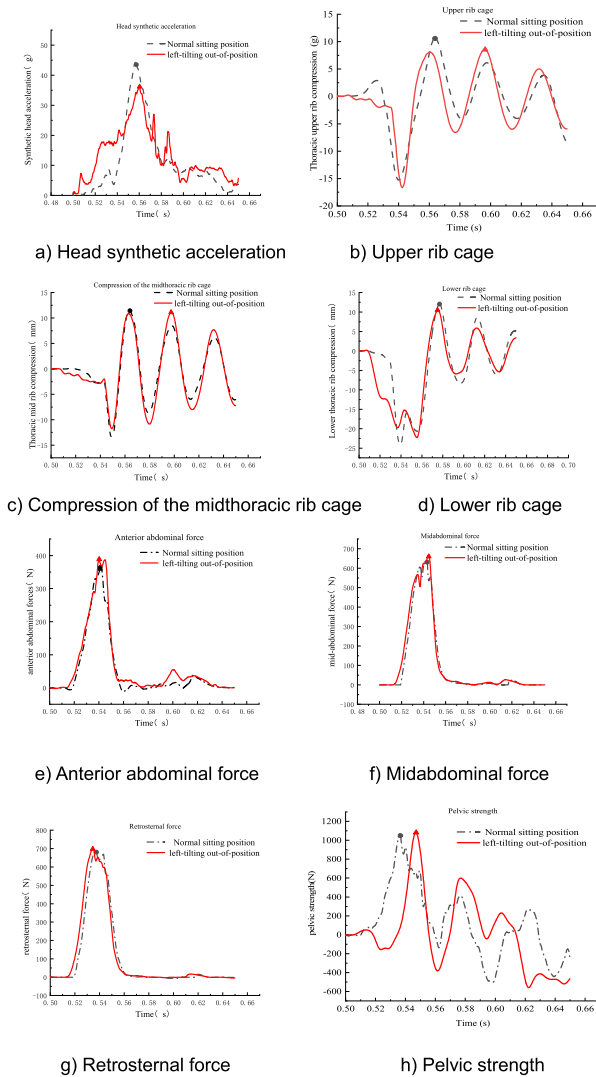
**TABLE 5. Collision response of dummies in different sitting positions.**

moment of collision	left-toward position	Normal sitting position
0ms		
60ms		
90ms		
150ms		

the upper rib cage were 15.17 mm and 0.18 m/s, respectively; the maximum compression and VC of the middle rib cage were 13.28 mm and 0.20 m/s, respectively; and the maximum compression and VC of the lower rib cage were 24.15 mm and 0.37 m/s, respectively. For the AES-induced leftward sitting position, the maximum compression and VC of the upper rib cage were 16.23 mm and 0.26 m/s, respectively; the maximum compression and VC of the middle rib cage were 11.68 mm and 0.15 m/s, respectively; and the maximum compression and VC of the lower rib cage were 22.05 mm and 0.18 m/s, respectively.

For the two sitting positions, the anterior abdominal force, midabdominal force, and posterior abdominal force of the dummy increased gradually, and the moments of peak force were all approximately 0.54 s. The peaks of the posterior and





**FIGURE 12.** Curves of injuries sustained by the dummy in various sitting positions.

anterior abdominal forces were highest and lowest, respectively, in both sitting positions. The main reason is that when the collision occurs, the handrail inside the left front door is at the same level as the abdomen of the dummy, so the handrail of the door is intruded by the impact force and squeezes the abdomen of the dummy, and the handrail inside the door squeezes the force of the dummy’s posterior abdomen more than that of the anterior abdomen. The combined abdominal force was 1698 N in the leftward sitting position and 1744 N in the normal sitting position. As displayed in Figure 12(h), although the peak values of the dummy pelvic force were similar between the leftward and normal sitting positions (1070 and 1083 N, respectively), these peaks appeared at different times. These similar values were attributed to the seatbelt effectively restraining the dummy’s pelvis during both collisions.

In summary, the postural response of the dummy’s torso during the collision differed considerably between the AES-induced leftward sitting position and the normal sitting

position. The most affected areas were the chest and abdomen of the dummy. The WIC values for the normal and leftward sitting positions were 0.492 and 0.407, respectively, a 17.28% decrease in WIC, indicating that the AES-induced leftward sitting position can reduce driver injury during a side impact.

**C. ANALYSIS OF DRIVER INJURIES FOR DIFFERENT IMPACT LOCATIONS**

The impact location of a side impact can also affect driver injury. Based on a comprehensive evaluation of side impact in the NAIS accident database, this study conducted collision simulations in which a moving barrier collided with the A-, B-, or C-pillar of the finite element model at a speed of 50 km/h; the study also considered the complexity of the actual road environment in the simulations. During a 90° collision with the moving barrier, the AES system caused the body of the vehicle to deflect, resulting in an angled collision.

During the collision, the two vehicles also moved forward. Therefore, to accurately simulate the vehicle kinematic responses before the two-car collision in HyperMesh, when setting the spacing of the two-vehicle pre-collision, it is offset by a certain distance from the original. Images of the vehicle kinematic responses for different impact locations are presented in Table 6.

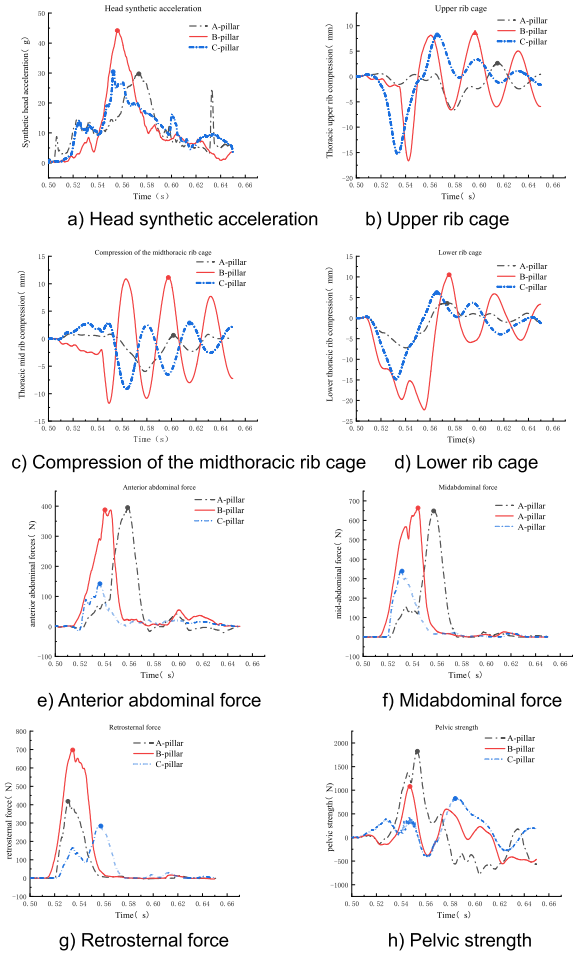
As indicated in this table, at the initial moment of the collision, the edge of the moving barrier was in contact with the A-, B-, or C-pillar. During the collision, both vehicles moved forward. For the A-pillar collision, the vehicle’s left-front fender, left-front wheels, A-pillar, left-front door, and left-front door sill beam all underwent deformation and intrusion. For the B-pillar collision, at the end of the collision, the parts with the greatest deformation were the B-pillar, the middle of the threshold beam, the left-front door, and the left-rear door. For the C-pillar collision, the parts with the greatest deformation were the left-rear C-pillar, the left-rear door, the left-rear side of the wing plate, and the left-rear wheel.

For a given simulation moment, the level of door intrusion differed between the three impact locations. For the A-pillar collision, the door exhibited partial intrusion, with the greatest level of intrusion occurring at the upper left side of the dummy pelvis. For the B-pillar collision, the entire left-side door intruded into the dummy’s space; consequently, the side airbag was squeezed by the door and the dummy simultaneously, resulting in its air pressure decreasing rapidly. For the C-pillar collision, the impact force was mainly concentrated at the left-rear door and the C-pillar. No internal intrusion occurred for the left-front door, and the dummy contacted the side air curtains and the side airbags due to inertia. The damage curves obtained for the dummy at the end of the collision for each part are presented in Figure 13.

The time and position at which the dummy head contacted the side air curtains also differed between the impact locations. As illustrated in Figure 13(a), the HIC values for the A-, B-, and C-pillar collisions were 85.88, 121.89, and 74.85, respectively. The impact speed was fixed in the simulations, and only the collision site was varied. The B-pillar was the

**TABLE 6.** Sequences of vehicle collision response for different impact locations.

A-pillar				
	0ms	30ms	60ms	
	90ms	120ms	150ms	
	B-pillar			
		0ms	30ms	60ms
90ms		120ms	150ms	
C-pillar				
		0ms	30ms	60ms
	90ms	120ms	150ms	



**FIGURE 13.** Curves of injuries sustained by the dummy for different impact locations.

the injury values for all three collision sites were less than the threshold values. Mainly due to the car-vehicle side impact speed is certain, only the collision site changes, the B-pillar from the driver’s dummy’s head is the closest, by the impact force is the largest, resulting in the impact of the B-pillar dummy’s head HIC value is the highest, but the dummy’s head with the side air curtains are beyond the protective range of the contact location and the side air curtains to expand to block the car window glass and car interiors and dummy’s head to occur a second collision. The upper, middle, and lower rib-cage compression values were similar for the three collisions; however, the B-pillar collision was associated with the highest lower rib-cage compression value. For the A-pillar collision, the maximum upper, middle, and lower rib-cage compression values occur at 0.54 to 0.58 ms. The maximum upper rib-cage compression and VC values were 6.5 mm and 0.0198 m/s, respectively; the maximum middle rib-cage compression and VC values were 5.9 mm and 0.0233 m/s, respectively; and the maximum lower rib-cage compression and VC values were 7.1 mm and 0.036 m/s, respectively. For the B-pillar collision, the maximum upper, middle, and lower rib-cage compression values occur at 0.54 to 0.56 ms. The maximum upper rib-cage compression and VC values

closest pillar to the head of the dummy; hence, the impact force and injury levels were greatest at this pillar. However,

were 16.23 mm and 0.26 m/s, respectively; the maximum middle rib-cage compression and VC values were 11.68 mm and 0.15 m/s, respectively; and the maximum lower rib-cage compression and VC values were 22.05 mm and 0.18 m/s, respectively. For the C-pillar collision, the maximum upper, middle, and lower rib-cage compression values occur at 0.53 to 0.56 ms. The maximum upper rib compression and VC values were 15.27 mm and 0.13 m/s, respectively; the maximum middle rib-cage compression and VC values were 9.15 mm and 0.06 m/s, respectively; and the maximum lower rib-cage compression and VC values were 22.05 mm and 0.18 m/s, respectively. These results indicate that VC is not always positively correlated with chest compression; it is also affected by the rate of chest deformation.

The peak values of the front abdominal force, midabdominal force, and rear abdominal force on the dummy for the different impact locations were observed at 0.52–0.58 ms into the collisions. The B-pillar collision was associated with the highest combined abdominal force (1698 N); those associated with the A-pillar and C-pillar collisions were 1332 and 906 N, respectively. In the collision between the moving barrier and the A-pillar, localized internal intrusion of the left front door occurred, with the first areas of compression being the pelvis and the left side of the abdomen; this explains why the abdominal force was higher for the A-pillar collision than it was for the C-pillar collision.

The magnitude and occurrence time of the peak pelvic force differed between the impact locations. For the A-pillar collision, the largest force was imposed on the pelvic bone (1827 N); in this collision, the worst area of door intrusion in a side impact is near the dummy's pelvic bone. For the B-pillar and C-pillar collisions, the forces acting on the dummy pelvic bone were 1070 and 1083 N, respectively.

In summary, the dummy's chest, abdomen, and pelvis were constrained by the seat belt in all collisions; therefore, the displacement of the dummy in the leftward OOP position did not vary considerably. The total injuries were mainly dependent on the survival space of the dummy. For the A-, B-, and C-pillar collisions, the WIC values were 0.230, 0.407, and 0.228, respectively. The WIC value increases and then decreases from the A-pillar to the C-pillar at the collision location, with the B-pillar having the highest WIC value and higher injury severity, and the C-pillar having the lowest and lower injury severity. When the collision position was column A, it caused an increase in the pelvic force of the dummy, which increased the risk of injury to the pelvis; when the collision position was column B, it caused an increase in the injury of the viscous index of the thorax and the combined force of the abdomen, which increased the risk of injury to the thorax and abdomen. The triggering of the AES changes the driver's survival space, and the above results lead to the conclusion that the closer the dummy was to the collision site, the smaller its survival space became and the greater the WIC value became. The deformation of the B-pillar increases the risk of occupant injury, so the AES system should be improved to avoid the collision of the B-pillar, and at the

same time with active pre-tensioning seat belts to enhance the protection ability of the restraint system and increase the survival space of the occupants.

#### D. EFFECT OF THE IMPACT ANGLE ON DRIVER INJURY










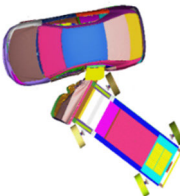
Most vehicle–vehicle side impacts do not occur at a 90° angle; an angle of deflection always exists when the collision initially occurs. The angle between the moving barrier and the vehicle model affected the damage and deformation sustained by the model. To further study the influence of angle change on side impact results, accordingly, this study conducted simulations of impact at angles of 60°, 75°, 90°, 105°, and 120°. To ensure the accuracy of the simulation experiment, in all simulations, the moving barrier impacted the same location on the vehicle and set the same simulation length; the displacements of the moving barrier during AES and the Initial position at the initial moment of the collision were estimated. The initial and postcrash deformations of the vehicle model at various impact angles are presented in Table 7.

The motion and deformation of the two vehicles during the impact differed considerably at various impact angles. For the impact at 60° and 75°, the front end of the vehicle model was deflected counterclockwise about the  $z$ -axis; this deflection was greater for the 60° impact. The most deformed parts of the vehicle model were the left-front door, B-pillar, and left door sill beam. For the 90° vertical impact, the entire vehicle model rotated counterclockwise about the  $z$ -axis, and the most deformed parts were the left-front door of the dummy, the left-front wing panel, the door sill beam, the B-pillar, and the left rear. For the 105° and 120° impacts, the entire vehicle model rotated counterclockwise about the  $z$ -axis; however, the offset of the rear part of the vehicle was greater than that observed in the other impact. The offset for the 105° impact was larger than that for the 120° impact; in both impacts, the most deformed parts were the left-front door, the B-pillar, the door sill beam, and the left-rear door. The movable barricade dolly was offset to the right during this collision and appeared to be fishtailing; a greater initial impact angle resulted in more severe fishtailing.

The impact angles also affected the intrusion of the left-front cab. As the deformations of the B-pillar and left front door increased, these parts exhibited greater levels of intrusion into the cab's safe space. The left-front door and B-pillar intrusions for different impact angles are illustrated in Figure 14 and Figure 15, respectively.

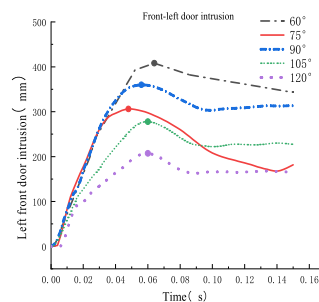
The maximum left-front door intrusion decreased as the impact angle increased, except for the 75° impact angle. For the 60°, 75°, 90°, 105°, and 120° impact, the maximum levels of intrusion of the left-front door were 408, 306, 359, 278, and 207 mm, respectively (Figure 14). In addition, as displayed in Figure 15, the maximum level of intrusion of the B-pillar decreased gradually as the impact angle increased, except for the 75° impact angle. For the 60°, 75°, 90°, 105°, and 120° impact, the maximum levels of intrusion of the B-pillar were 362, 290, 311, 265, and 207 mm, respectively. In summary,

**TABLE 7. Vehicle deformation for different impact angles.**

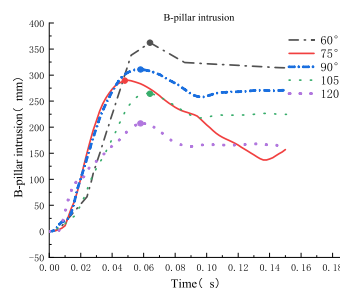
	The initial moment of collision	Deformation of the whole vehicle after the collision
impact angle 60°		
impact angle 75°		
impact angle 90°		
impact angle 105°		
impact angle 120°		

the impact angles associated with the maximum levels of intrusion of the left-front door and B-pillar can be ordered as follows (in descending order): 60°, 90°, 75°, 105°, and 120°. Figure 16 presents the curves of injuries sustained by the dummy.

The finite element model of the vehicle was equipped with side airbags, side air curtains, and seat belts to protect the occupants. The AES-induced rightward steering of the vehicle resulted in a leftward OOP response in the driver. The peak head synthetic acceleration varied for the different impact angles but was always less than the threshold value;



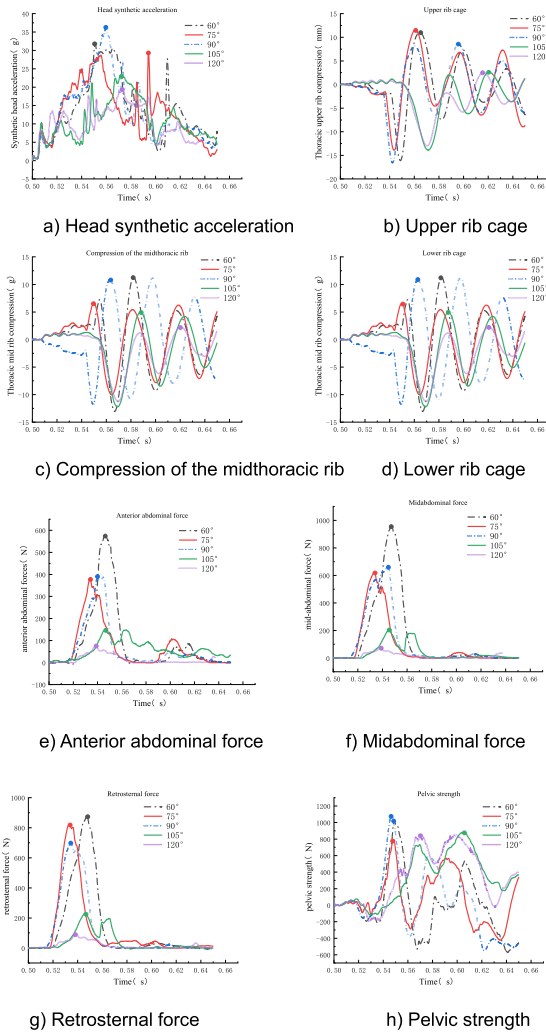
**FIGURE 14. Front-left door intrusion**



**FIGURE 15. B-pillar intrusion**

the largest (36g) occurred for the 90° impact angle. For the 60°, 75°, 90°, 105°, and 120° impact, the HIC values were 105, 91, 121, 55, and 35, respectively, all of which were also less than the threshold value. The main reason is that the side collision of the mobile barrier vehicle speed is the same, in the AES role of the dummy leftward OOP response is the same, although different angles of the collision on the driving space invasion amount are different, due to the vehicle model and the mobile barrier as a whole lower, the collision area is concentrated in the dummy torso, the collision occurs in the collision, the side of the air curtains are normally inflatable to unfold the head of the dummy is completely subjected to the constraints of the curtains, and did not have a secondary collision with the interior decoration of the car and the car window glass.

The upper, middle, and lower rib-cage compression curves were similar for all impact angles. The maximum chest compression observed for the 105° and 120° impact were smaller than those observed for the 60°, 75°, and 90° impact. For the 60°, 75°, and 90° impacts, the most severe deformation occurred at the left-front door and the B-pillar (the closest part to the dummy); for the 105° and 120° impacts, the most severe deformation occurred at the left-rear door and the B-pillar. For the 60°, 75°, and 90° impact, the lower rib cage had the highest level of compression, and for the 105° and 120° impact, the upper rib cage had the highest level of compression. For the 105° and 120° impacts, the impact force was mainly concentrated in the front of the left-rear door, but no direct intrusion into the dummy’s torso was observed; therefore, the compression was smaller. This was attributed to the deployed side air curtains contacting the dummy’s left upper arm, further squeezing the upper rib cage. According



**FIGURE 16.** Curves of injuries sustained by the dummy for different impact angles.

to Table 8, for the 60°, 75°, 90°, 105°, and 120° impact, the maximum compression values for the ribs were 24.07, 22.03, 22.05, 13.89, and 13.02 mm (a gradually decreasing trend), respectively, and the VCs were 0.23, 0.22, 0.18, 0.08, 0.06 m/s, respectively. The risk of chest injury increases with decreasing angle of impact, with a potential risk of injury to the dummy chest at 60°. VC was not proportional to chest compression primarily because VC is related to the rate of chest deformation. The maximum chest compression was less than the threshold value of 42 mm specified in FMVSS208, and the chest viscosity index was also less than the threshold value of 1.0 m/s specified in regulations. The driver’s maximum chest compression and chest viscosity index at different angles were within the threshold values and did not cause serious injury to the chest.

The front, center, and rear abdominal forces generally decreased as the impact angle increased. Changes in impact angle caused the risk of abdominal injuries, with smaller impact angles increasing the risk of abdominal injuries, which provides a better understanding of the changes in the risk of

**TABLE 8.** Dummy thorax compression at different impact angles.

impact angle	Maximum compression of the upper ribs of the chest (mm)	Maximum compression of mid-thoracic ribs (mm)	Maximum compression of the lower ribs of the chest (mm)
60°	21.21	18.44	24.07
75°	13.78	10.01	22.03
90°	16.23	11.68	22.05
105°	13.89	12.21	8.79
120°	13.02	11.32	9.25

injuries to the vehicle and driver in an accident, implying that the driver has the lowest risk of abdominal injuries in a 120° collision. Moreover, the front and rear abdominal forces were typically the smallest and largest, respectively. Depending on the characteristics of the rear abdominal forces, this risk of injury can be reduced with an active pre-tensioned seat belt. The combined abdominal forces for the 60°, 75°, 90°, 105°, and 120° impacts were 2638, 1823, 1744, 581, and 238 N, respectively. The European ECER95 Regulation states that the combined abdominal force should not exceed 2500 N; however, the combined abdominal force for the 60° impact was noted to exceed this threshold. Therefore measures such as optimizing AES systems or improving seat belts need to be considered to avoid excessive driver injuries.

The dummy posture was noted to be consistent among the side impacts occurring at various angles because of the seat belt restraint. The damage to the dummy was generally inversely correlated with the distance between the dummy and the part of the vehicle model into which the moving barrier intruded. The WIC values for the 60°, 75°, 90°, 105°, and 120° impact were 0.485, 0.393, 0.408, 0.200, and 0.158, respectively. From the WIC values, it can be seen that the most severe driver injury and abdominal synergy exceeds the threshold value at impact angle of 60°, whereas the WIC values for impact angles of 105° and 120° are relatively small, and changing the impact angle has the greatest effect on the abdomen, increasing the risk of injury to the abdomen. Based on these results, the AES cornering can be optimized and the vehicle can be fitted with active pre-tensioner seat belts to reduce the severity of the driver’s injuries.

**E. ANALYSIS OF DRIVER INJURY UNDER ACTIVE SEAT BELT PRE-TENSIONING**

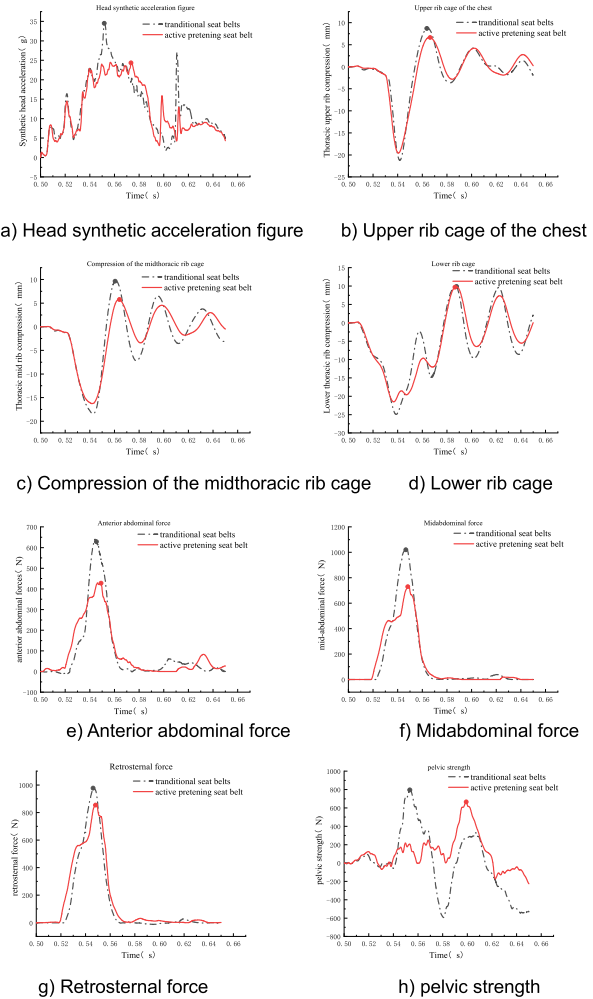
Active seat belt pre-tensioning systems have been proposed by researchers for effectively restraining drivers during collision avoidance and to increase driver protection in the event of a collision [27]. The triggering principle of the active pre-tensioning seat belt is to trigger the motor of the active

pre-tensioning retractor immediately after detecting the danger by the vehicle’s own sensors, and then the motor drives the turbine worm gear to make the retractor retract the seat belt, thus realizing the pre-tensioning in advance. In the event of a collision, a better angle and distance, in conjunction with the airbag deployment angle, can minimize occupant damage. To study the effect of active seat belt pre-tensioning systems on driver displacement and injury during AES actions, this study included an active seat belt pre-tensioning system in the finite element model and compared its effects with those of traditional seat belts under various driver lateral accelerations. The maximum decrease in the side displacement of the dummy under each lateral acceleration is listed in Table 9.

**TABLE 9. The dummy’s maximum decrease in side displacement for different lateral accelerations with the active seat belt.**

lateral accelerations	Maximum drop in head	Maximum neck drop	Maximum chest drop	Maximum pelvic drop
0.3g	60.2%	71.9%	65.9%	74.3%
0.4g	52.9%	62.1%	53.5%	60.9%
0.5g	47.8%	55.1%	43.9%	56.3%
0.6g	15.5%	19.8%	16.6%	50.4%

Compared with the traditional seat belts, the active seat belt pre-tensioning system reduced the dummy’s displacement under all lateral accelerations, but its effectiveness varied under the various accelerations. As listed in Table 9, the active seat belt pre-tensioning system was most effective in reducing the displacement of the neck and pelvis. Active pre-tensioner seat belts restrain the dummy best in lateral OOP when the lateral acceleration is 0.3g, 0.4g, and 0.5g. This is because the vehicle’s steering acceleration is small, and the dummy is subjected to less lateral inertia force, which leads to a smaller amount of lateral dislocation, the active pre-tensioning seat belts in the pre-crash phase after the role of a force opposite to the direction of the occupant’s movement will be applied to constrain the occupant’s lateral dislocation. As the lateral acceleration was increased, the restraining effect of the active pre-tensioning system decreased. Larger lateral accelerations can invalidate the protection of the restraint system as well as challenge vehicle stability, and AES system improvements cannot be considered to reduce occupant injury severity by increasing lateral acceleration alone. the system was least effective at a lateral acceleration of 0.6g, at which the pre-tensioning force before the collision was no longer sufficient to prevent dummy displacement. Accordingly, this study compared the damage sustained by the dummy when the active pre-tensioning system was used with the damage sustained when the traditional seat belts were used under a lateral acceleration of 0.6g.



**FIGURE 17. Injuries sustained by the dummy using traditional seat belts and active seat belt pre-tensioning.**

As displayed in Figure 17, when the active seat belt pre-tensioning system was used, the synthetic acceleration of the dummy’s head was 24.5g, and the HIC was 83; this was 20.9% lower than that observed when the traditional seat belts were used (HIC of 105). Moreover, the compression of the upper, middle, and lower rib cages decreased from 21.21 to 19.55 (7.8%), 18.44 to 16.26 (11.8%), and 24.07 to 21.51 mm (10.6%), respectively, when the active seat belt pre-tensioning system was used. Similarly, the active seat belt pre-tensioning system reduced the anterior abdominal, midabdominal, and posterior abdominal forces from 638 to 427 N (33.1%), 1022 to 710 N (30.5%), and 978 to 864 N (11.6%), respectively. The pelvic bone force also decreased from 1022 to 798 N (21.9%). Therefore, the active seat belt pre-tensioning system considerably reduced the dummy injury values for the head, abdomen, and pelvis; a smaller amount also reduced chest injury values. This is because restraining the dummy out of position under the action of an active pre-tensioning seat belt also alters the optimum protective properties of the restraint system; Secondly, the active pre-tensioning seat belts mainly consider restraining the longitudinal displacement of

the driver, to a certain extent, ignoring the potential risk of lateral displacement of the driver to the driver, inherently in the optimization of the restraining system should be taken into account in the role of the auxiliary driving functions such as the AES system. The intervention of active seat belts reduces the severity of driver injuries to a certain extent, and the combination of the AES system with the restraint system can better protect the safety of the occupants. Improvement and optimization should not be detached from the vehicle system itself, but need to take into account the comprehensive consideration of the assisted driving function, which is a great improvement to improve the whole driver safety protection system.

**IV. DISCUSSION**

This study established an AES control algorithm, simulation scenarios, and a whole-vehicle model and analyzed the dynamic OOP response of the driver under various lateral accelerations. Different steering accelerations cause different driver displacements, and the driver’s displacement may influence the effectiveness of the in-vehicle restraint system during the collision. Therefore, analyzing the effect of displacement on driver injury is crucial for improving driver protection. The largest OOP was observed at a lateral acceleration of 0.6g. Hence, this study investigated driver injury for different seating postures under this lateral acceleration and comprehensively assessed the damage to the dummy. In general, driver injuries can be reduced by AES, and including an active seat belt pre-tensioning system can further improve safety. Although passive safety clearly reduces the degree of driver injury, the results of this study indicate that both active and passive safety systems should still be further optimized. This study bridges the gap in research on vehicle–vehicle side impact in scenarios that involve AES systems and provides supporting data for optimizing AES systems.

**TABLE 10. Orthogonal test factors and values.**

level	Ignition moment	Vent area B	Mass flow rate
	A		C
1	-3	0.8	0.8
2	6	1	1
3	+3	1.2	1.2

Research has found that left OOP reduces the severity of driver injuries, Zhe et al. [11] studied the forward disengagement of occupants caused by the AEB system, and Mages et al. [16] showed that this disengagement increases occupant injuries, so we believe that excessive disengagement will cause the driver to come into contact with the door or the B-pillar, which will increase the risk of driver injuries, and that, in addition to the improvement of the AES system, it is necessary to match the active pre-tensioning seat belts with

the side airbags to protect the driver; More serious damage occurred when the collision area was the B-pillar, and Prochowski et al. [28] also indicated that contact with the B-pillar caused the most serious damage in a side impact; At impact angle of 60°, the abdominal combined force was found to exceed the threshold and the severity of injury was higher, so we suggest that improvements to the AES need to be made to avoid the B-pillar and impact angles of 60° as much as possible. With active pre-tensioning seat belts, lateral OOP of all parts of the driver was reduced, and driver injuries were reduced compared to normal seat belts. As lateral acceleration increases, active pre-tensioning seat belt pre-tensioning force underperforms and restraint capacity decreases. The risk of abdominal injuries was not significantly reduced, considering that the active pre-tensioning seatbelt mainly restrains lateral displacements, and the restraining process increases abdominal pressure, so the AES system and the active pre-tensioning seatbelt need to be improved for the abdomen, to further restrain lateral displacements and reduce the risk of abdominal injury. When the collision cannot be avoided, the results of the study can be used to optimize the setting of the optimal collision pattern to reduce the degree of driver injury. In addition to the several factors considered in this paper, other factors should not be ignored, for example, lateral acceleration affects the longitudinal stability of the vehicle, which may cause rollover in the event of a collision; the AES system alters the angle of the steering wheel of the vehicle, and the rotational speed of the steering wheel may also pose a potential risk to the driver.

Imler et al. [29] investigated the effects of relative speed, restraint systems, and occupant position on occupant injuries in vehicle–vehicle side impact; they revealed that occupants wearing seat belts sustained fewer injuries than those who did not wear seat belts. Dong et al. [30] examined the motion and intrusion velocity of doors during side impact and established a side impact dolly model with dummies; the dummy damage sustained in the dolly test and the actual side impact test results were highly correlated. Moreover, Yanchao et al. [31] explored the head and torso injuries sustained by occupants sitting in various positions on the side of a vehicle that was impacted during a side impact; they demonstrated that if the occupants rotated to the right side, head and torso injuries were minimized, but clavicle injuries were maximized. However, none of these studies on side impact have considered the effects of AES systems. Unlike previous side-impact studies, we considered vehicle-vehicle side-impacts under the effect of AES, which causes driver OOP and can change the driver’s injury risk, and it is important for driver protection to explore the driver’s injury under the OOP response.

Shang et al. [32] investigated the acceleration profile of a dummy’s chest in frontal crash tests and found that active seat belt pre-tensioning along with emergency braking systems increased the risk of chest injury. The present study also observed that active seat belt pre-tensioning did not significantly reduce dummy chest injuries. To effectively protect drivers and reduce the risk of chest injuries during a collision,

**TABLE 11. Orthogonal test data sheet.**

Experiment number	Ignition moment A	Vent area B	Mass flow rate C	Maximum compression of thoracic ribs (mm)	Chest Viscosity Index VC (m/s)	Abdominal force synergy (N)	pelvic strength (N)	WIC value
1	-3	0.8	0.8	21.03	0.203	2228	593	0.409
2	-3	1	1	18.06	0.082	1560	654	0.300
3	-3	1.2	1.2	21.89	0.16	1751	614	0.365
4	6	0.8	1	24.24	0.20	1666	509	0.385
5	6	1	1.2	23.10	0.18	1427	504	0.350
6	6	1.2	0.8	15.89	0.14	2390	537	0.365
7	+3	0.8	1.2	23.57	0.12	1536	495	0.343
8	+3	1	0.8	17.35	0.10	2215	577	0.350
9	+3	1.2	1	19.41	0.20	1958	651	0.377

this study proposes measures for optimizing the design of side airbags. Specifically, drivers can be effectively protected by appropriately setting the airbag deployment time, vent area, and mass flow rate. For side impact, the time before the side airbags deployment should be reduced; this study determined the optimal deployment time to be 6 ms. This study optimized the performance of the side airbags of the occupant restraint system by conducting an orthogonal test with three factors, namely deployment time, vent area, and mass flow rate, at three levels. HyperMesh was used to investigate the effect of the three factors on airbag performance: the value of the vent area coefficient curve of the side airbag was set to 0.8, 1, and 1.2; the airbag deployment delay time was set to -3, 0, and 3 ms; and the values of the gas mass flow rate of the airbag were set to 0.8, 1, and 1.2 (Table 10). Therefore, nine simulations were performed by the orthogonal method.

WIC values were derived to determine injuries sustained by the dummy in the simulations (Table 11).

Extreme value analysis was conducted to investigate the extent to which the factors at the three levels influenced the WIC; the analysis results are presented in Table 12, where levels 1, 2, and 3 indicate the average WIC values for the corresponding factors. As indicated in Table 12, factors affecting the performance of the side airbags could be ordered as follows (in descending order): vent area, mass flow rate, and deployment time. The optimal combination was determined to be A3B2C3, which was based on the average of the WIC values for each factor at each level.

The WIC and other injury criteria for the side airbags with optimized parameters were determined and compared with those obtained before optimization to validate the results.

Optimizing the side airbags significantly reduced injury for all parts of the dummy. The HIC decreased from 83 to 58

**TABLE 12. Range analysis table.**

	Ignition moment A	Vent area B	Mass flow rate C
Level 1	0.358	0.379	0.375
Level 2	0.367	0.333	0.377
Level 3	0.357	0.369	0.354
extreme value	0.01	0.046	0.023
optimal combination	3	2	3

(30.1%), and the chest viscosity index, pelvic forces, abdominal combined force, and maximum rib-cage compression were reduced by 41.2%, 34.3%, 23.7%, and 17.8%, respectively. The driver is closer to the collision vehicle in a side impact than in a frontal impact, and only the side airbags, side air curtains, and side door parts can absorb the collision energy. Therefore, to further protect occupants, the side parts of the car, as well as the interior trim, should be upgraded and optimized.

Regarding the errors and limitations, considering that the local structure and material properties of the model and the actual situation are not the same, and to reduce the model computing time, the mesh division of the model is larger, and the size of the mesh has a certain impact on the subsequent analysis, which causes errors in modeling and analysis, and through the subsequent validation of the model, it is shown that the errors are all within the controllable range. This study



**TABLE 13. Injury criteria for the optimized and unoptimized side airbags.**

	Large compression of the ribs in the chest (mm)	Chest Viscosity Index VC (m/s)	Combine d- abdominal force (N)	pelvic strength (N)	WIC value
pre- optimization	21.51	0.17	2001	798	0.391
post- optimization	17.69	0.10	1527	524	0.295
decline	17.8%	41.2%	23.7%	34.3%	24.6%

has some limitations: Only one ES-2re dummy model was used, and only upper-body injuries in side impact were studied. Injuries to the leg were not investigated. Hence, future studies should consider using other dummies to investigate leg injuries. Moreover, only driver injuries were studied; rear occupants are not as well protected and could have different injuries. Therefore, future studies should explore injuries sustained by rear occupants during collisions.

## V. CONCLUSION

This study conducted simulations by considering both active and passive safety technology to investigate driver injuries caused by side impact in scenarios in which a suddenly appearing vehicle was occluded from the field of view of the vehicle's AES system. We established a precrash scenario by using PreScan, developed an AES control algorithm in MATLAB, and obtained vehicle dynamics by using CarSim. A joint simulation was then performed to extract the lateral acceleration trajectory of the vehicle during the steering process, and the extracted trajectory data were subsequently used to establish a finite element model of the vehicle by using HyperWorks. In HyperWorks, the finite element model was subjected to side impact, and the driver OOP responses were studied under different lateral accelerations before the collisions. The integration of AES systems with active and passive safety technologies is emphasized. Providing case-specific parameters on how to better integrate these technologies to improve overall vehicle safety can make the findings more operational and practically instructive, helping to drive the automotive safety industry in the direction of safer and smarter vehicles. The results reveal that greater lateral accelerations were associated with greater driver head, neck, and chest displacements. Moreover, based on the OOP response data, the risk of injury for drivers in different sitting positions was studied. The results indicate that the AES-induced leftward sitting position was associated with fewer injuries than the normal sitting position. Furthermore, injuries sustained by the driver at different impact locations and impact angles

were also investigated. For B-pillar (closest to the driver) collisions, driver head, chest, and abdomen injuries were the most severe. Driver injury typically depends on the size of the survival space. The study determined that as the impact angle was increased, the levels of intrusion of both the door and the B-pillar gradually decreased. Differences in driver head, chest, abdominal, and pelvic injuries were small, but the injuries increased as the impact angle decreased; 60° impact was associated with the most severe injuries. In particular, this study determined that the abdominal force sustained during the collisions exceeded the threshold value at this angle, indicating that further safety optimization is required. Finally, when an active seat belt pre-tensioning system was included in the model, dummy head, abdominal, and pelvic injury values were considerably reduced when compared with those observed when traditional seat belts were used; chest injuries were also moderately reduced when this system was used. The research will contribute to a more comprehensive understanding of the impact of AES systems on vehicle safety in real-world driving, providing valuable insights for system improvement and future vehicle design. Presenting the results of the study to provide a basis for the development of relevant regulations and policies to ensure the safety and compliance of automated driving systems, as well as training and awareness-raising measures to improve the proper use and understanding of AES systems by drivers to maximize their potential benefits. For foreseeable collisions, the AES system can adjust the impact angle, collision position, and other parameters through the vehicle position to plan the path with optimal decision-making.

## REFERENCES

- [1] J. Kovaceva, A. Bálint, R. Schindler, and A. Schneider, "Safety benefit assessment of autonomous emergency braking and steering systems for the protection of cyclists and pedestrians based on a combination of computer simulation and real-world test results," *Accident Anal. Prevention*, vol. 136, Mar. 2020, Art. no. 105352, doi: [10.1016/j.aap.2019.105352](https://doi.org/10.1016/j.aap.2019.105352).
- [2] P. Castaing, P. Shaw, M. Goyens, and T. Van Esbroeck. (2017). *Euro NCAP Roadmap-2025-v4*. [EB/OL]. [Online]. Available: <https://cdn.euroncap.com/media/30700>
- [3] A. Eskandarian, *Handbook of Intelligent Vehicles*. London, U.K.: Springer, 2012, doi: [10.1007/978-0-85729-085-4](https://doi.org/10.1007/978-0-85729-085-4).
- [4] W. Haibin, "Research on vehicle emergency collision avoidance algorithm," M.S. thesis, School Energy Eng., Power Eng., Zhejiang Univ., Zhejiang, China, 2020.
- [5] K. Liufu, Q. Liu, Y. Lu, Z. Chen, Z. Zhang, and Q. Li, "Multi-objective optimization on cooperative control of autonomous emergency steering and occupant restraint system for enhancing occupant safety," *Accident Anal. Prevention*, vol. 159, Sep. 2021, Art. no. 106302, doi: [10.1016/j.aap.2021.106302](https://doi.org/10.1016/j.aap.2021.106302).
- [6] A. J. McNeill, J. Haberl, M. Holzner, R. Schoeneburg, T. Strutz, and U. Tautenhahn, "Current worldwide side impact activities—Divergence versus harmonisation and the possible effect on future car design," in *Proc. 19th Int. Tech. Conf. Enhanced Saf. Vehicles (ESV)*, Jun. 2005, Paper 05-0077.
- [7] *Annual Report of the People's Republic of China on Road Traffic Accident Statistics*, Traffic Management Bureau of the Ministry of Public Security, Beijing, China, 2015. [Online]. Available: <http://data.stats.gov.cn/search.htm?s=>
- [8] M. Gidlewski, L. Prochowski, L. Jemioł, and D. Dardecki, "The process of front-to-side collision of motor vehicles in terms of energy balance," *Nonlinear Dyn.*, vol. 97, no. 3, pp. 1877–1893, Dec. 2018, doi: [10.1007/s11071-018-4688-x](https://doi.org/10.1007/s11071-018-4688-x).

- [9] S. Battaglia, K. Kietlinski, M. Unger, and R. Bours, "Occupant behavior during a one-lane change maneuver resulting from autonomous emergency steering," in *Proc. Int. Tech. Conf. Enhanc. Saf. Veh (ESV) Nat. Highway Traffic Saf. Admin.*, Jan. 2013, pp. 1–13.
- [10] C. Jiang, X. Meng, L. Ren, X. Liu, and C. Li, "Relevance analysis of AEB control strategy and occupant kinematics based on typical cut-in scenario," *Int. J. Crashworthiness*, vol. 27, no. 1, pp. 198–205, Jul. 2020, doi: [10.1080/13588265.2020.1785099](https://doi.org/10.1080/13588265.2020.1785099).
- [11] X. Zhe, L. Lei, G. Guanyu, and W. Xu, "Occupant protection performance affected by the combination of autonomous emergency braking and reversible pretension seatbelt," *Auto Time*, vol. 2, pp. 188–192, Jan. 2021.
- [12] Li Wei, W. Jing, and D. Jianmin, "Polynomial-based lane-changing trajectory planning for intelligent vehicles," *Comput. Eng. Appl.*, vol. 48, no. 3, pp. 242–245, 2012.
- [13] R. Bis, H. Peng, and A. G. Ulsoy, "Vehicle occupancy space for unmanned ground vehicles with actuation error," *Int. J. Vehicle Auto. Syst.*, vol. 12, no. 2, p. 180, 2014, doi: [10.1504/ijvas.2014.060115](https://doi.org/10.1504/ijvas.2014.060115).
- [14] S. Yang, "Quantitative evaluation of intelligence levels for unmanned ground vehicles," Ph.D. dissertation, School Mech. Vehicles, Mech. Eng., Beijing Inst. Technol., Beijing, China, 2014.
- [15] J. Suh, H. Chae, and K. Yi, "Stochastic model-predictive control for lane change decision of automated driving vehicles," *IEEE Trans. Veh. Technol.*, vol. 67, no. 6, pp. 4771–4782, Jun. 2018, doi: [10.1109/TVT.2018.2804891](https://doi.org/10.1109/TVT.2018.2804891).
- [16] M. Mages, M. Seyffert, and U. Class, "Analysis of the pre-crash benefit of reversible belt pre-pretensioning in different accident scenarios," in *Proc. 22nd Int. Tech. Conf. Enhanced Saf. Vehicles (ESV) Nat. Highway Traffic Saf. Admin.*, Jan. 2011, Paper 11-0442.
- [17] S. Xiao, J. Wu, J. Hou, F. Mo, Z. Liu, W. Ma, and H. Zhang, "Analysis of chest response characters for drivers in lateral and oblique automotive impact," *Int. J. Crashworthiness*, vol. 28, no. 1, pp. 46–54, May 2022, doi: [10.1080/13588265.2022.2074631](https://doi.org/10.1080/13588265.2022.2074631).
- [18] L. Fei, H. Chaoqun, D. Hongliang, C. Tao, and Z. Shulian, "Research on automatic emergency collision avoidance of intelligent vehicle in extreme condition by combined braking and steering control," *Automot. Eng.*, vol. 43, no. 6, pp. 851–860, 2021, doi: [10.19562/j.chinasae.qcgc.2021.06.008](https://doi.org/10.19562/j.chinasae.qcgc.2021.06.008).
- [19] H. Yoshida, S. Shinohara, and M. Nagai, "Lane change steering manoeuvre using model predictive control theory," *Vehicle Syst. Dyn.*, vol. 46, no. 1, pp. 669–681, Sep. 2008, doi: [10.1080/00423110802033072](https://doi.org/10.1080/00423110802033072).
- [20] *LS-DYNA Keyword User's Manual*, Livermore Software Technol. Corporation, Livermore, CA, USA, 2003.
- [21] Q. Shah, "LS-DYNA para principiantes," Novas Edições Acadêmicas, Amazon, Tech. Rep., Jan. 2022.
- [22] D. C. Viano and S. Arepally, "Assessing the safety performance of occupant restraint systems," in *Proc. SAE Technical Paper Series*, Oct. 1990, p. 7191, doi: [10.4271/902328](https://doi.org/10.4271/902328).
- [23] W. Cong, "Design method and analysis for the configurations of adaptive occupant restraint system," M.S. thesis, Mech. Eng., Tsinghua Univ., Beijing, China, 2012. [Online]. Available: <https://kns.cnki.net/KCMS/detail/detail.aspx?dbname=CMFD2012&filename=1011280870.nh>
- [24] X. Lingyun, H. Wenhao, W. Yan, W. Xiaobo, and D. Honglei, *Comparative Analysis of Vehicle Accident In-Depth Investigation Technology Between China and Germany*. Beijing, China: China National Institute of Standardization (CNIS), 2018. [Online]. Available: <https://kns.cnki.net/KCMS/detail/detail.aspx?dbname=SNAD&filename=SNAD000001966355>
- [25] D. Smith and J. M. Starkey, "Overview of vehicle models, dynamics, and control applied to automated vehicles," *Adv. Automot. Technol.*, pp. 69–87, Jan. 1991.
- [26] N. H. Sledge, "An investigation of vehicle critical speed and its influence on lane-change trajectories," Ph.D. dissertation, Dept. Mech. Eng., Univ. Texas, Austin, TX, USA, 1997.
- [27] C. Libo, O. Zhigao, G. Kang, and C. Kai, "The implementation of control system for active pre-tensioning safety belt," *Automobile Eng.*, vol. 38, no. 11, pp. 1300–1304+1299, 2016, doi: [10.19562/j.chinasae.qcgc.2016.11.004](https://doi.org/10.19562/j.chinasae.qcgc.2016.11.004).
- [28] L. Prochowski, M. Ziubiński, K. Dziejewski, and P. Szwajkowski, "Impact energy and the risk of injury to motorcar occupants in the front-to-side vehicle collision," *Nonlinear Dyn.*, vol. 110, no. 4, pp. 3333–3354, Aug. 2022, doi: [10.1007/s11071-022-07779-8](https://doi.org/10.1007/s11071-022-07779-8).
- [29] S. Imler, M. Heller, C. Corrigan, K. Zhao, and H. Watson, "The effect of side impact collision delta-V, restraint status, and occupant position on injury outcome," SAE Tech. Paper 2010-01-1158, Apr. 2010, doi: [10.4271/2010-01-1158](https://doi.org/10.4271/2010-01-1158).
- [30] L. P. Dong, X. C. Zhu, and Z. X. Ma, "Side impact sled test method based on multipoint impact," *J. Tongji Univ.*, vol. 43, no. 8, pp. 1213–1218, 2015.
- [31] X. Yanchao, X. Sen, C. Yong, C. Guang, and Q. Zhidong, "Study on injury distribution of the mechanical dummy based on side-collision," *J. Mach. Des.*, vol. 37, no. 1, pp. 21–25, 2020, doi: [10.13841/j.cnki.jxsj.2020.01.004](https://doi.org/10.13841/j.cnki.jxsj.2020.01.004).
- [32] E.-Y. Shang, D.-Y. Zhou, and Y.-M. Li, "Research on abnormal problems of the Q3 Dummy's chest acceleration curve in frontal crash test," *Automob. Technol.*, vol. 20, no. 3, pp. 45–49, 2020.



**CHENGLONG ZHANG** was born in Sichuan, China, in 1998. He is currently pursuing the master's degree with Xihua University, Chengdu, China.

His research interest includes traffic safety.



**XIAOYAN LI** was born in Nanchong, Sichuan, China, in 1996. She received the master's degree in transportation from Xihua University, Chengdu, China, in 2023.

She is currently a Research and Development Member of Chengdu Metro Operation Company. Her research interests include vehicle active and passive safety.



**YI LEI** was born in Sichuan, China, in 1995. He is currently pursuing the master's degree with Xihua University, Chengdu, China.

His research interests include vehicle active and passive safety.



**DAOWEN ZHANG** was born in Mianyang, Sichuan, China. He received the master's degree in mechanical manufacturing and automation from Sichuan University, in 2002.

He is currently a Professor with Xihua University, Chengdu, China. His current research interests include automotive safety, utilization engineering, and road traffic safety.



**TIANSHU ZHANG** was born in Sichuan, China, in 1998. He is currently pursuing the master's degree with The University of Adelaide, Australia. His research interest includes engineering.

• • •